Published in final edited form as:
Biomaterials. 2011 September ; 32(26): 6245–6253. doi:10.1016/j.biomaterials.2011.05.004.

Magnetically-Enabled and MR-Monitored Selective Brain Tumor Protein Delivery in Rats via Magnetic Nanocarriers

Beata Chertok[1,4], **Allan E. David**[1,2], and **Victor C. Yang**[1,3,*]

[1]Department of Pharmaceutical Sciences, College of Pharmacy, University of Michigan, Ann Arbor, Michigan 48109, USA

[2]ISTN Inc., York, PA 17404, USA

[3]School of Pharmacy, Tianjin Medical University, Tianjin 300072, China

Abstract

The delivery of bioactive proteins to tumors is associated with many difficulties that have impeded clinical translation of these promising therapeutics. Herein we present an approach, including (1) use of magnetically-responsive and MRI-visible nanoparticles as drug carriers, (2) topography-optimized intra-arterial magnetic targeting, (3) MRI-guided subject alignment within the magnetic field, and (4) surface modification of the protein drug with membrane-permeable polyethyleneimine (PEI), to prevail over the obstacles in protein delivery. Applying these methodologies, we demonstrated the delivery of a significant quantity of β-Galactosidase selectively into brain tumors of glioma-bearing rats, while limiting the exposure of normal brain regions. Clinical viability of the technologies utilized, and the ability to deliver proteins at high nanomolar-range tumor concentrations, sufficient to completely eradicate a tumor lesion with existing picomolar-potency protein toxins, renders the prospect of enabling protein-based cancer therapy extremely promising.

1. Introduction

Cancer is among the world's top killers [1]. Despite several decades of effort, treatment options have seen only modest improvements. This is especially true of brain tumors, which have proven refractory to all current therapies [2]. In fact, due to the ineffective treatments, many brain tumor patients receive only symptomatic care to ease end-of-life. The need for more efficacious therapy is clearly acute.

A major challenge for brain tumor treatment includes its deep seating within the brain – surrounded by function-critical brain parenchyma [2]. While direct brain intervention (e.g. surgery, intra-tumoral injections) poses risks of impairing surrounding normal tissues that carry vital brain functions, radiation therapy can cause tissue damage along its path to the tumor site. Chemotherapy, on the other hand, has contributed very little to improving

*Correspondence and reprint requests should be addressed to: Victor C. Yang, Ph.D., Albert B. Prescott Professor of Pharmaceutical Sciences, College of Pharmacy, University of Michigan, Ann Arbor, Michigan 48109-1065, Tel: (734) 764-4273, Fax: (734) 763-9772, vcyang@umich.edu.
[4]Present address: Department of Chemical Engineering, Massachusetts Institute of Technology, Cambridge, Massachusetts 02139, USA

survival time due to the low potency of existing small molecule drugs and toxic effects caused by a lack of target specificity [3].

Proteins, with unparalleled substrate specificity [4], low susceptibility to multi-drug resistance[5], and exquisitely high potency[6] constitute an emerging class of promising therapeutics for cancer treatment. Many potent tumor suppressor proteins (e.g. p53), chemotherapeutic prodrug activating enzymes (e.g. cytosine deaminase) and anti-neoplastic enzymes (e.g. arginine deaminase) have already been developed [7–9] and the advents in genomics, recombinant technology and protein engineering are expected to further expand the arsenal of proteins for combating cancer. Despite this remarkable potential, the clinical translation of potential protein therapeutics faces a bottleneck. Instability in circulation due to proteolytic degradation and inability to permeate through biological membranes [4] hamper their efficacy. While protein translocation across the blood-brain-barrier (BBB) can be enhanced through covalent conjugation with polycationic molecules (e.g. HIV-TAT, polyethyleneimine; PEI)[10–12], this approach lacks tumor selectivity and exposes normal tissues to the cytotoxic effects of the agent. In view of these problems, we attempted the development of a non-brain-invasive, tumor-selective delivery system for protein drugs using magnetic nanotechnology.

The underlying concept is simple. Protein drugs are modified with polycationic PEI domains to enable translocation across biological membranes and then electrostatically loaded onto heparin-coated iron-oxide nanoparticles. Selective localization of the drug-loaded nanoparticles is then achieved via use of an externally induced magnetic flux gradient. We previously demonstrated the feasibility of achieving a magnetically-mediated retention of superparamagnetic nanoparticles within tumor lesions of orthotopic glioma-bearing rats[13]. Nonetheless, extension of this methodology to protein delivery still faces a host of challenges that have yet to be solved.

Passive delivery of magnetic nano-carriers to the tumor microvasculature is required for their magnetic capture. However, the positive surface charge, imparted by PEI modification, leads to extremely short circulation half-lives and negligible tumor exposure [14, 15]. To this regard, intra-arterial administration via carotid artery could provide a clinically viable route to bypass the first pass systemic clearance and enhance nanoparticle exposure of the tumor vasculature [16], thereby facilitating magnetic capture. Unfortunately, arterial embolization [17] due to magnetically-induced nanoparticle aggregation has undermined the usefulness of this method thus far.

In the present study, we sought to develop an integrative methodology for tumor delivery of a cationized model protein β-Galactosidase (β-Gal) in orthotopic-glioma-bearing rats. We hypothesized that heparin-coated superparamagnetic nanoparticles could be utilized as a delivery platform for cationized proteins. We further hypothesized that an integrative intra-arterial magnetic targeting methodology combining: 1) optimization of magnetic field topography; 2) MRI-guided subject alignment within the field; and 3) preservation of physiological arterial hydrodynamics during nanocarrier administation would allow embolization-free and tumor-selective delivery of protein-impregnated nanocarriers to brain tumor lesions.

2. Materials and Methods

2.1 Materials

Iron oxide nanoparticles coated with heparin (GHep) were generously contributed by Chemicell ® (Berlin, Germany). βGalactosidase, Poly(ethylenimine) (MW ~ 1200) and

chlorophenol red β-D-galactopyranoside (CPRG) were obtained from Sigma; 1-Ethyl-3-[3-dimethylaminopropyl] carbodiimide Hydrochloride (EDC) was purchased from Pierce.

2.2 In Vitro Studies

2.2.1 Coupling of PEI to β-Galactosidase—The surface of β-Galactosidase (β-Gal) was chemically modified with short-chain polyethylenimine (PEI) using EDC-mediated coupling procedure as previously described [11]. Briefly, βGal was dissolved at a concentration of 1 mg/ml in PEI solution (60 mg/ml, pH 6). The reaction was initiated by adding EDC to the protein solution to a final concentration of 0.5 mg/ml. The reaction mixture was stirred for 48 hours at 4°C. The cationized protein (βGal-PEI) was first purified by ultrafiltration using 10 kDa molecular weight cut-off membrane (Millipore) to completely remove unreacted PEI. The conjugate was further purified by cation-exchange chromatography on Hi-Trap Heparin column (GE Healthcare Life Sciences, Piscataway, NJ). The cationized protein, in contrast to the original β-Gal, exhibited strong affinity for the heparin column. A fraction of the loaded conjugate, which required 2M NaCl for elution from the heparin column, was collected, desalted and used for further experiments.

2.2.2 Loading of β-Gal-PEI on GHep Nanoparticles—The complexation of βGal-PEI with GHep nanoparticles was studied by mixing different amounts of βGal-PEI, in the range of 0–25 μg protein, with 200 μg GHep and then diluting to a total volume of 500 μL with deionized water. The mixtures were incubated for 30 minutes at RT, followed by isolation of the complexes using a magnetic separator. Zeta potential and particle size distribution of the purified complexes were measured with Nicomp 380/ZLC size/zeta potential analyzer (Nicomp, Santa Barbara, CA).

To elucidate the βGal-PEI loading capacity of GHep nanoparticles, GHep (200 μg) was incubated with an excess of βGal-PEI (25 μg). Following 30 minutes incubation at RT, the nanoparticles were immobilized using a magnetic separator and the supernatant isolated and analyzed for protein content using the bicinchoninic acid (BCA) protein assay (Thermo Fisher Scientific Inc., Rockford, IL).

2.3 *In Vivo* Studies

All animal experiments were conducted according to the protocols approved by the University of Michigan Committee on Use and Care of Animals (UCUCA).

2.3.1 Induction of Brain Tumors—Intracerebral 9L tumors were induced in male Fisher 344 rats weighting 125–150 g according to a previously described procedure [18]. Briefly, rat 9L-glioma cells (Brain Tumor Research Center, University of California, San Francisco) were cultured in Dulbecco's modified Eagle's medium (DMEM) supplemented with 10% heat-inactivated fetal bovine serum, 100 IU/mL penicillin, 100 μg/mL streptomycin and 0.29 mg of L-glutamine at 37°C in a humidified atmosphere of 5% CO_2. Prior to implantation, cells were grown to confluence in 100 mm culture dishes, harvested and resuspended in serum free DMEM at a concentration of ~10^5 cells/μL. The cell suspension (10 μL) was implanted in the right forebrain of the animals at a depth of 3 mm beneath the skull through a 1-mm-diameter burr hole. The surgical field was cleaned with 70% ethanol and the burr hole was filled with bone wax (Ethicon Inc., Summerfield, NJ) to prevent extracerebral extension of the tumor. The tumor volume of the animals was monitored with MRI beginning on day 10 after cell implantation to select tumors with volumes between 70 and 90 μL for magnetic targeting experiments.

2.3.2 Magnetic Resonance Imaging—MRI experiments were performed on an 18-cm horizontal-bore, 7 Tesla Varian Unity Inova imaging system (Varian, Palo Alto, CA).

Animals were anesthetized with 1.5% isoflurane/air mixture and imaged using a 35-mm-diameter quadrature RF head coil (USA Instruments Inc, OH). To visualize the tumor localization within the rat brain, 13 axial sections of the brain were acquired with a T_2-weighted fast spin echo sequence using the following parameters: repetition time (TR) = 4 s, echo time (TE) = 60 ms, field of view = 30 × 30 over 128 × 128 matrix, slice thickness = 1 mm, slice separation = 2 mm, four signal averages per phase encoding step. Longitudinal and lateral location of the tumor lesion relative to the middle of the eye and the midline of the head, respectively, was calculated using the acquired images. Animal heads were marked with MRI-derived tumor coordinates to allow precise positioning of the animals within the targeting magnetic field. To determine nanoparticle distribution in the brain, 13 gradient echo (GE) axial slices of the brain were collected before the nanoparticle administration (baseline scans) and immediately following magnetic targeting. GE images were acquired with the following parameters: TR = 20 ms, TE = 5 ms, field of view = 30 × 30 over 128 × 128 matrix, slice thickness = 1mm.

2.3.4 Magnetic Targeting—For magnetic targeting studies, the right carotid artery of glioma-bearing animals was catheterized as previously described [19]. Briefly, the right carotid artery of anaesthetized animals was exposed by blunt dissection. The catheter composed of silica capillary tubing and PE-10 tubing was inserted cephalad through the arterial wall. The tiny incision was rapidly resealed with a drop of tissue adhesive (3M Vetbond), allowing to maintain intact blood flow through the catheterized artery.

The configuration of the magnetic setup and the animal positioning with respect to the magnet were optimized to direct the highest magnetic force towards the targeted tumor region. The magnetic setup consisted of a small cylindrical ferromagnet mounted on the tapered pole of the standard dipole electromagnet (GMW Associates, Model 3470). The magnetic flux density was measured using a teslameter (MetroLab THM 7025 model, GMW Associates, San Carlos, CA) equipped with a three-dimensional Hall sensor. The topographic maps of magnetic flux density were plotted using MathCad11 software package (Mathsoft Inc., MA).

The rats were placed supinely on the platform. The animal heads, marked with MRI-derived coordinates of the glioma lesion, were positioned according to the mapped magnetic field topography to align the tumor with the peak field density and gradient.

The magnetic field density at the pole face of the ferromagnet was adjusted to 0 (control) or 350 mT (experimental). The animals were injected with βGal-PEI/GHep complexes at a dose of 1.8 mg protein [and 12 mg Fe]/kg via catheterized carotid artery and retained in magnetic field for 30 min. The rats were imaged with MRI before the administration of nanoparticles and after the magnetic targeting as described above. Immediately following MRI, the rats were transcardially perfused to clear the brain of its blood content. The animals were infused with 200 ml of an ice-cold Phosphate Buffered Saline (PBS) through the left ventricle at a flow rate of 30 ml/min. After perfusion, the animals were dissected and the isolated brain divided into right and left hemispheres. The tumor was carefully separated from the normal tissue of the right hemisphere. The left hemisphere and the tumor tissues were frozen and kept at −80°C. For βGal histochemistry, tissue segments were frozen in Tissue-Tek O.C.T. embedding medium (Sakura Finetek, Torrance, CA) and stored at −80°C until sectioning.

2.4 *Ex vivo* analysis of tissue samples

2.4.1 Analysis of βGal Activity in Tissue Samples—βGal activity in excised tissue samples was assayed by a spectrophotometric method using chlorophenol red β-D-galactopyranoside (CPRG) as a substrate. The experimental conditions, minimizing the

background of endogenous βGal activity, were adapted from a previously described protocol [20] with some modifications. Tissue samples (~50 mg) were homogenized on ice in 50 μL lysis buffer (Tropix Inc., Bedford, MA) using a pestle tissue grinder. The homogenates were diluted with 950 μL of 100 mM buffer HEPES (pH 7) also containing 100 mM KCL and 1 mM $MgSO_4$. After adding 2 μL of 0.28 M CPRG solution, the samples were incubated at 37°C for 1 hour. Immediately following incubation, the reaction mixture was centrifuged at 10,000 rpm for 5 minutes. The supernatant was separated and its optical density analyzed on a microplate reader (Power-Wave 340, Bio-Tek Instruments, Winooski, VT) at 575 nm. One unit of βGal activity (U) was defined as the amount of enzyme releasing one μmole of chlorophenol red per minute at pH 7 and 37°C. A calibration curve with chrolorophenol red (optical density versus concentration) was constructed to calculate the βGal activity of tissue samples from their measured optical density. The calibration curve was linear (R^2=0.998) within the range of 0–8 nmol chlorophenol red. To reduce the endogenous tissue background, βGal activity was also measured in tissue samples of control rats, not exposed to the exogenous enzyme. The control enzymatic activity was subtracted from the activities measured in experimental samples.

2.4.2 Histochemical Analysis of Excised Brain Tissues—Frozen tissue blocks were sectioned at 12-μm thickness on a cryostat (Microm, HM500M, GMI Inc., MN) and the sections mounted on microscope slides (Superfrost Plus, Fisherbrand). The frozen sections were fixed with 10% formaldehyde solution for 2 minutes, washed in DW and incubated with 5-bromo-4-chloro-3-indoyl-β-D-galactoside (X-Gal) staining solution (BetaBlue Staining Kit, Novagen, NJ, USA) at 37°C overnight.

For capillary visualization, X-Gal stained sections were incubated with Burstone's reagent at 37°C for 1 hour. The sections were then washed with DW, cover-slipped using 50% glycerol in PBS solution and imaged with light microscopy.

2.5 Statistical analysis

Data are presented as mean ± SE, unless indicated otherwise. SPSS 16.0 statistical software package (SPSS Inc., Chicago, IL) was used for data analysis. βGal activities in excised tumor, contralateral and ipsilateral brain tissues were compared using one-way analysis of variance (ANOVA), followed by Tukey's multiple comparisons test. A p-value of <0.05 was considered statistically significant.

3. Results and Discussion

3.1 Development of methodology for selective magnetic targeting of brain tumor lesions

To facilitate tumor-selective delivery of magnetic nanoparticles while avoiding arterial embolization, we first attempted to control the interplay of major forces that contribute to magnetic entrapment. As known, intravascularly-administered superparamagnetic nanoparticles are convectively transported by the blood flow. When exposed to a magnetic flux density gradient, nanoparticles magnetize, thus developing a net magnetic moment, and experience a force of magnetic attraction. This magnetic force acts to capture the nanoparticles from the flowing blood and is opposed by the hydrodynamic drag force, which strives to propel the particles in the direction of the flow. Hence, we hypothesized that nanoparticle entrapment in the tumor vascular bed and afferent arterial vasculature could be differentiated by regulation of flow dynamics and design of optimized magnetic flux topography.

Our previous studies using an *in vitro* flow model revealed that under constant magnetic flux and gradient conditions, the entrapment of magnetic nanoparticles from the flowing fluid

diminished with increasing linear flow velocities [21]. To maximize the flow rate through carotid artery, we employed a cannulation methodology which did not require vessel occlusion – maintaining physiological blood flow in the afferent arterial vasculature during intra-arterial nanoparticle administration. In addition, we designed a magnetic force field with a steep gradient which would peak at the tumor location and rapidly decay towards the carotid injection site. Objectives of this design were two-fold: (1) to minimize the magnetic force applied to the carotid injection site, $\bar{F}m(carotid)$, relative to the local hydrodynamic drag force, $\bar{F}h(carotid)$, such that arterial nanoparticle entrapment is avoided; and (2) to generate a sufficiently high magnetic force at the tumor site, $\bar{F}m(tumor)$, capable of overcoming the drag force in the tumor vascular bed, $\bar{F}h(tumor)$, and enable target site capture. To identify an easily realizable magnet configuration which would satisfy the design objectives (Eq.1 & Eq.2), we simulated magnetic force fields acting on a single nanoparticle with different magnet configurations (detailed description of the force field simulations can be found in Supplementary Information).

$$\overline{F}m(carotid)/\overline{F}h(carotid)<1 \quad [1]$$

$$\overline{F}m(tumor)/\overline{F}h(tumor)>1 \quad [2]$$

Components chosen for simulation analysis were limited to those readily available for implementation in our laboratory and included a dipole electromagnet and a set of permanent magnets of variable geometry and strength. The magnetic forces at the peak and at the distance of 2.5 cm from the peak, which approximately corresponded to the location of common carotid artery in 200 g Fisher 344 rats, were compared to the calculated hydrodynamic drag force acting on a single nanoparticle in the tumor capillary and carotid artery, respectively. As seen in Figure 1, a dipole electromagnet, which was used in previous studies for brain tumor magnetic targeting [22], produced a homogeneous broad-range magnetic flux topography (Figure 1A & B), resulting in a shallow force field gradient that was unable to satisfy the criteria of Equations 1 and 2 (Figure 1C). Indeed, as seen in Table 1, the ratio of $\bar{F}m(carotid)/\bar{F}h(carotid)$ was found to be 2.7 (>1), suggesting carotid retention of the nanoparticles. In sharp contrast, an optimized magnet configuration, which was adopted using force field simulations, resulted in a focused magnetic flux topography (Figure 1D & E) and steep force field gradient (Figure 1F). In this magnet configuration, a small cylindrical magnet (9 mm in diameter) was placed on the tapered electromagnet pole. The magnetic force field of this configuration indeed satisfied the design criteria of Equations 1 & 2, as the ratios of $\bar{F}m(carotid)/\bar{F}h(carotid)$ and $\bar{F}m(tumor)/\bar{F}h(tumor)$were found to be 0.4 (<1) and 1.8 (>1), respectively (see Table 1), suggesting no nanoparticle entrapment in the carotid artery as opposed to that at the target tumor site.

3.2 Loading of PEI-Modified β-Gal on the Surface of Magnetic Nanoparticles

We next attempted to utilize magnetic nanoparticles as a carrier for brain tumor protein delivery. β-Galactosidase (β-Gal), selected as the model protein due to ease of detection *ex vivo*, was conjugated with low molecular weight cationic polyethyleneimine (PEI, ~1200 Da) chains to produce cationized β-Gal (β-Gal-PEI) possessing the desirable membrane-permeable functions. Due to the presence of oppositely charged polyelectrolyte heparin on the nanoparticle surface, β-Gal-PEI could be electrostatically, and reversibly, loaded onto the heparin-coated nanoparticle (GHep), as schematically depicted in Figure 2A. Measurements of ζ-potential of GHep nanoparticles mixed with different concentrations of β-Gal-PEI (Figure 2Ba) revealed that the negative surface charge of GHep (ζ-potential = −33 mV) was progressively masked with increasing concentrations of β-Gal-PEI,

confirming successful electrostatic complexation. For example, at the loading ratio of 7.5% w/w (β-Gal-PEI/GHep), the particles were found to exhibit positive ζ-potential of +24 mV (Figure 2Bb). DLS analysis further demonstrated that the hydrodynamic diameter of the nanoparticles increased from ~122 nm for GHep to ~176 nm for GHep mixed with β-Gal-PEI at a ratio of 7.5% w/w (Figure 2C). Since β-Gal is a large tetrameric protein (hydrodynamic diameter of ~16 nm[23]), the increase in nanoparticle size is obviously due to the complexation of β-Gal-PEI to GHep.

The ζ-potential profile (Figure 2Ba) exhibited saturation behavior, as no further increase in ζ-potential could be reached beyond the loading ratio of 7.5% w/w (β-Gal-PEI / GHep). This behavior reflected attainment of the protein loading capacity. Analysis of the content of the nanoparticle-loaded protein also revealed a loading capacity of 7.2 ± 0.4% w/w for the β-Gal-PEI/GHep complexes, consistent with the ζ-potential results. Interestingly, with our simple loading method, a significantly higher β-Gal loading capacity was obtained on magnetic nanoparticles compared with the literature reported value for β-Gal on PLGA microspheres (2.8 ± 0.16 % w/w[24]), the most commonly used carriers for protein compounds to-date. This finding underscores the value of nanoparticles as carriers for therapeutic compounds, due to their unmatched surface-to-volume ratios thereby permitting an exceedingly high surface-loading of bioactive agents. Since the loading ratio of 7.5% w/w β-Gal-PEI/GHep constituted the maximal protein loading per nanoparticle weight this formulation was used for the β-Gal-PEI/GHep complex for all subsequent studies, unless otherwise stated.

The β-Gal-PEI conjugates loaded onto GHep was found to exhibit a specific activity of 533 ± 53 mU/mg protein. Given that the dose of magnetic nanoparticles typically administered to rats is 12 mg Fe/kg (~24 mg particles/kg), the β-Gal-PEI/GHep loading ratio is 7.5% w/w, and the rat weight is 200 g, the activity of β-Gal that could be administered to a single rat was estimated to be approximately 190 mU. Considering that the endogenous background of β-Gal activity of the tumor is about 500 nU/mg tissue, administration of 190 mU of β-Gal per rat allowed a reliable detection of 0.02% of the administered dose in a 50 mg tumor tissue sample. Hence, we found the specific activity of the GHep-adsorbed β-Gal to be adequate for the planned *in vivo* feasibility study.

Examination of the magnetic properties of β-Gal-PEI/GHep complexes revealed that they exhibit superparamagnetic behavior, as the induced magnetization curves displayed neither hysteresis nor remanent magnetization (Figure 2D). A high saturation magnetization of 108 emu/g Fe suggested that the protein-loaded nanoparticles would be amenable to magnetic targeting.

3.3 Magnetic Delivery of β-Gal-PEI/GHep Complexes to Brain Tumor Lesions

We next assessed the feasibility of delivering the PEI-modified β-Gal to brain tumor lesions using GHep as the delivery platform and employing the optimized magnetic setup. To fully utilize the benefits of the focused magnetic flux, we also sought to align the tumor lesion with the region of the maximal magnetic flux density by proper positioning of a rat with respect to the magnetic setup. For realization of such positioning we used MR imaging to determine the intracerebral localization of the tumor lesion, based on the fact that the tumor can be clearly visualized as a hyperintense region on T_2-weighted MRI scans. As seen in Figure 3, acquisition of 12 axial slices of the animal head allowed mapping of the tumor lesion location with respect to externally visible anatomical features of the animal head such as the center of the eye (Figure 3A) and the midline of the head (3B).

Using the MRI-derived tumor coordinates, we positioned the rat with respect to the magnetic setup in a way that maximized the alignment of the tumor lesion with the peak of

the magnetic flux density (Figure 3C). The magnetic nanoparticles (starch-coated, $\zeta = -12$ mV) were then injected via a non-occlusively cannulated carotid artery. Localization of magnetic nanoparticles was examined with MRI, as the presence of magnetic nanoparticles at a particular spatial location could be easily visualized by resulting hypointensity (negative contrast) on gradient echo (GE) MRI images.

As shown in Figure 4A, in the absence of magnetic targeting, no clear difference could be visually discerned between the post-targeting and the baseline GE MRI brain scans of animals administered with either the free β-Gal-PEI conjugates or the β-Gal-PEI / GHep complexes; suggesting the lack of nanoparticle entrapment in the tumor. In sharp contrast, with magnetic targeting, the GE post-targeting scan of complex-administered animal showed a region of pronounced hypointensity. Importantly, this region spatially corresponded to the location of the tumor lesion (hyperintense region on the T_2-weighted baseline scan), confirming a markedly augmented accumulation of magnetic nanoparticles selectively at the targeted tumor site.

To further evaluate brain distribution of the delivered β-Gal, we analyzed β-Gal activity in the excised tumor, and contra-lateral and ipsilateral normal brain tissues (Figure 4B). As seen, in the absence of magnetic targeting, no significant difference in β-Gal activity ($p = 0.596$) was detected between the tumor, contra-lateral and ipsilateral regions of the brain following administration of either the free β-Gal-PEI conjugates or the β-Gal-PEI / GHep complexes. In contrast, tumors of magnetically-targeted rats displayed significantly higher β-Gal activity ($p < 0.001$) than that in the control tissues. In particular, following administration of the protein-loaded nanoparticles, 4.7-fold higher β-Gal activity ($p < 0.001$) was detected in tumors of the targeted rats (636 ± 42 μU/g tissue) than that in the non-targeted animals (134 ± 46 μU/g tissue), demonstrating viability of the developed magnetic targeting method in delivering a functional protein to the tumor target. Most importantly, pronounced tumor selectivity of protein localization was observed in targeted animals, as tumor tissues displayed 7.5-folds higher β-Gal activity (636 ± 42 μU/g tissue, $p < 0.001$) than the contra-lateral normal brain tissues (85 ± 30 μU/g tissue), as well as 6.3-fold higher activity than the ipsilateral normal brain tissues (101 ± 30 μU/g tissue; $p < 0.001$).

Histochemical examination, for β-Gal activity, of frozen brain sections from magnetically targeted rats provided further evidence of the specific and extensive deposition of β-Gal in the tumor (Figure 5A), but not in the ipsilateral (Figure 5B) and contra-lateral normal brain regions (Figure 5C); firmly corroborating tumor-selective protein delivery by magnetic targeting. Furthermore, co-staining of the targeted tumor sections with both Burstone's (capillary visualization) and X-Gal (β-Gal visualization) reagents revealed lack of overlap of these two stains, suggesting that β-Gal was indeed delivered into the parenchyma of the tumor and not confined to the microvasculature (Figure 5D–F). At this moment, the mechanism of β-Gal delivery to the tumor parenchyma still remains unclear. Translocation of cationized proteins across endothelial lining via absorptive-mediated transcytosis has been previously reported[12]. Literature evidence also suggests that electrostatic binding between PEI and heparin is likely to be reversible in plasma [25]. Therefore, it is possible that following tumor localization of the β-Gal-PEI / GHep complexes by magnetic targeting, PEI-β-Gal conjugates gradually desorb from the GHep carrier and subsequently cross the microvascular barrier via PEI-mediated transcytosis. Another possibility is the delivery of entire β-Gal-PEI / GHep complexes into tumor parenchyma due to the PEI-covered surfaces which may confer membrane-translocating ability. Further examination of this phenomenon, however, is necessary to elucidate its mechanism. Regardless, the results corroborate the accomplishment of highly selective delivery of the very large β-Gal protein into tumor parenchyma. Importantly, the quantity of protein delivered to the tumor is very much therapeutically relevant, as the achieved tumor concentration of β-Gal (2.6 nM, see

Supporting Information) is about 100-fold higher than reported IC_{50} values for existing anti-neoplastic proteins (e.g. chimeric toxin IL13-PE38QQR, IC_{50} < 20 pM[26]), found to effectively eradicate glioma cells *in vitro*.

Results presented in this paper demonstrate the selective delivery of a therapeutic concentration of functionally-active protein into a brain tumor lesion, but not the normal brain parenchyma, via a non-brain-invasive method. The only other report on successful delivery of a meaningful level of β-Gal into the brain parenchyma came from Dowdey and co-workers, who achieved delivery with the aid of a potent protein transduction domain (PTD) peptide (i.e. HIV-TAT) [10]. However, due to the lack of selectivity of the TAT peptide, a widespread and non-specific distribution of β-Gal was observed throughout the entire brain, compromising its clinical applicability for treating brain cancers due to potential severe drug-associated systemic and brain toxicity. Moreover, while this previous method required administration of 40–200 nmol/kg of the TAT-β-Gal conjugates to attain a detectable level of β-Gal in the brain [10], our method facilitated β-Gal accumulation in the brain tumor with a dose as low as only 4 nmol/kg - a remarkable 10–50 fold dose reduction. It should be pointed out that β-Gal is one of the largest known tetrameric enzymes (MW = 465 kDa), and thus its successful and selective tumor delivery suggests the potential for applying this drug delivery methodology to a wide variety of protein therapeutics. Moreover, the facile nanocarrier loading method may enable the co-delivery of a macromolecular drug cocktail for robust combined chemotherapy.

Lastly, most components of the described brain tumor protein delivery system are feasible for clinical translation. Iron-oxide based magnetic nanoparticles were previously reported to be safe [17, 27, 28], and have been clinically employed as MR contrast agents for over a decade [29]. In addition, carotid catheterization constitutes a clinically viable procedure which can be performed with minimally invasive endovascular technology [30, 31]. MRI-guided patient positioning based on accurate topographic definition of intra-cerebral tumor lesions is already being utilized in stereotactic radiotherapy [32, 33]. At present, the only technological limitation for application of the described methodology in humans is unavailability of the high-gradient magnets that would be able to retain magnetic nanoparticles within deep-seated brain tumor lesions (about 8–10 cm from the surface in adults). Nevertheless, rapid development of high-gradient superconducting magnets is anticipated to overcome this shortcoming in the near future, since magnets that can capture moving magnetic nanoparticles at a 2-cm distance from the magnet surface have already been reported [34]. To this regard, our methodology offers a promising avenue for expanding the clinical utilization of protein therapeutics to combat brain cancer in the foreseeable future. The potential impact and clinical significance of this brain drug delivery system is therefore far-reaching.

4. Conclusions

By applying an integrative delivery approach combining (1) the use of MRI-visible magnetic nanoparticles as the drug carrier; (2) topography-optimized intra-arterial magnetic targeting to bypass the first-pass organ clearance of the nanoparticles; (3) MRI-guided subject alignment within the magnetic field, and (4) surface modification of the protein drug with biological membrane-permeable PEI, we successfully demonstrated, in a rat glioma model, the delivery of a significant quantity of β-Galactosidase selectively into a brain tumor, while limiting the exposure of normal brain regions. With most of the technologies involved being feasible for clinical translation, and exquisitely potent protein toxins already available, the prospect of achieving a clinically viable brain tumor protein therapy is extremely promising.

Supplementary Material

Refer to Web version on PubMed Central for supplementary material.

Acknowledgments

We thank Dr. Christian Bergemann from Chemicell (Germany) for the generous gift of iron oxide nanoparticles. We acknowledge the Center for Molecular Imaging at the University of Michigan for providing access to the MRI facility. This work was supported in part by NIH RO1 Grants CA114612 and NS066945, as well as a research grant from the Hartwell Foundation. This research was also partially sponsored by Grant R31-2008-000-10103-01 from the World Class University (WCU) project of the MEST and NRF of South Korea. Victor C. Yang is currently a Participating Faculty in the Department of Molecular Medicine and Biopharmaceutical Sciences, College of Medicine & College of Pharmacy, Seoul National University, South Korea. In, addition, the project was partially sponsored by the National Basic Research Program of China (973 Program) 2007CB935800. Beata Chertok was a recipient of the University of Michigan Rackham Graduate School Pre-doctoral Fellowship.

References

1. Jemal A, Siegel R, Xu J, Ward E. Cancer statistics, 2010. CA Cancer J. Clin. 60(5):277–300. [PubMed: 20610543]
2. Louis DN, Posner JB, Jacobs T, Kaplan R. Report of the brain tumor progress review group. NIH Publication number 01–4902. 2000
3. DeAngelis LM. Chemotherapy for brain tumors - A new beginning. N. Engl. J. Med. 2005; 352(10): 1036–1038. [PubMed: 15758016]
4. Leader B, Baca QJ, Golan DE. Protein therapeutics: a summary and pharmacological classification. Nat. Rev. Drug. Discov. 2008; 7(1):21–39. [PubMed: 18097458]
5. Liu TF, Cohen KA, Willingham MC, Tatter SB, Puri RK, Frankel AE. Combination fusion protein therapy of refractory brain tumors: demonstration of efficacy in cell culture. J. Neurooncol. 2003; 65(1):77–85. [PubMed: 14649887]
6. Yamaizumi M, Mekada E, Uchida T, Okada Y. One molecule of diphtheria toxin fragment A introduced into a cell can kill the cell. Cell. 1978; 15(1):245–250. [PubMed: 699044]
7. Michiue H, Tomizawa K, Matsushita M, Tamiya T, Lu YF, Ichikawa T, et al. Ubiquitination-resistant p53 protein transduction therapy facilitates anti-cancer effect on the growth of human malignant glioma cells. FEBS Lett. 2005; 579(18):3965–3969. [PubMed: 15996664]
8. Vellard M. The enzyme as drug: application of enzymes as pharmaceuticals. Curr Opin Biotechnol. 2003; 14(4):444–450. [PubMed: 12943856]
9. Rooseboom M, Commandeur JN, Vermeulen NP. Enzyme-catalyzed activation of anticancer prodrugs. Pharmacol Rev. 2004; 56(1):53–102. [PubMed: 15001663]
10. Schwarze SR, Ho A, Vocero-Akbani A, Dowdy SF. In vivo protein transduction: delivery of a biologically active protein into the mouse. Science. 1999; 285(5433):1569–1572. [PubMed: 10477521]
11. Futami J, Kitazoe M, Maeda T, Nukui E, Sakaguchi M, Kosaka J, et al. Intracellular delivery of proteins into mammalian living cells by polyethylenimine-cationization. J. Biosci. Bioeng. 2005; 99(2):95–103. [PubMed: 16233763]
12. Bickel U, Yoshikawa T, Pardridge WM. Delivery of peptides and proteins through the blood-brain barrier. Adv. Drug Delivery Rev. 1993; 10:205–245.
13. Chertok B, Moffat B, David A, Yu F, Bergemann C, Ross B, et al. Iron oxide nanoparticles as a drug delivery vehicle for MRI monitored magnetic targeting of brain tumors. Biomaterials. 2008; 29(4):487–496. [PubMed: 17964647]
14. Papisov M, Bogdanov A, Schaffer B, Nossiff N, Shen T, Weissleder R, et al. Colloidal magnetic-resonance contrast agents - effect of particle surface on biodistribution. J. Magn. Magn. Mater. 1993; 122(1–3):383–386.
15. Chertok B, David AE, Yang VC. Polyethyleneimine-modified iron oxide nanoparticles for brain tumor drug delivery using magnetic targeting and intra-carotid administration. Biomaterials. 2010; 31(24):6317–6324. [PubMed: 20494439]

16. Groothuis DR. The blood-brain and blood-tumor barriers: a review of strategies for increasing drug delivery. Neuro-Oncol. 2000; 2(1):45–59. [PubMed: 11302254]

17. Lubbe AS, Bergemann C, Huhnt W, Fricke T, Riess H, Brock JW, et al. Preclinical experiences with magnetic drug targeting: tolerance and efficacy. Cancer Res. 1996; 56(20):4694–4701. [PubMed: 8840986]

18. Ross BD, Zhao Y-J, Neal ER, Stegman LD, Ercolani M, Ben-Yoseph O, et al. Contributions of cell kill and posttreatment tumor growth rates to the repopulation of intracerebral 9L tumors after chemotherapy: an MRI study. Proc. Natl. Acad. Sci. USA. 1998; 95:7012–7017. [PubMed: 9618530]

19. Rodriguez M, Barroso N. An improved method for carotid artery infusion without vessel occlusion. Physiol. Behav. 1992; 52(6):1211–1213. [PubMed: 1484883]

20. Young DC, Kingsley SD, Ryan KA, Dutko FJ. Selective inactivation of eukaryotic beta-galactosidase in assays for inhibitors of HIV-1 TAT using bacterial beta-galactosidase as a reporter enzyme. Anal. Biochem. 1993; 215(1):24–30. [PubMed: 8297011]

21. Chertok B, David AE, Huang Y, Yang VC. Glioma selectivity of magnetically targeted nanoparticles: a role of abnormal tumor hydrodynamics. J. Control. Release. 2007; 122(3):315–323. [PubMed: 17628157]

22. Pulfer SK, Ciccotto SL, Gallo JM. Distribution of small magnetic particles in brain tumor-bearing rats. J. Neurooncol. 1999; 41(2):99–105. [PubMed: 10222429]

23. Sutter M, Oliveira S, Sanders NN, Lucas B, van Hoek A, Hink MA, et al. Sensitive spectroscopic detection of large and denatured protein aggregates in solution by use of the fluorescent dye Nile red. J. Fluoresc. 2007; 17(2):181–192. [PubMed: 17294134]

24. Stivaktakis N, Nikou K, Panagi Z, Beletsi A, Leondiadis L, Avgoustakis K. Immune responses in mice of beta-galactosidase adsorbed or encapsulated in poly(lactic acid) and poly(lactic-co-glycolic acid) microspheres. J. Biomed. Mater. Res. A. 2005; 73(3):332–338. [PubMed: 15793820]

25. Yang T, Hussain A, Bai S, Khalil IA, Harashima H, Ahsan F. Positively charged polyethylenimines enhance nasal absorption of the negatively charged drug, low molecular weight heparin. J. Control. Release. 2006; 115(3):289–297. [PubMed: 17023085]

26. Husain SR, Puri RK. Interleukin-13 receptor-directed cytotoxin for malignant glioma therapy: from bench to bedside. J. Neurooncol. 2003; 65(1):37–48. [PubMed: 14649884]

27. Lubbe AS, Bergemann C, Riess H, Schriever F, Reichardt P, Possinger K, et al. Clinical experiences with magnetic drug targeting: a phase I study with 4'-epidoxorubicin in 14 patients with advanced solid tumors. Cancer Res. 1996; 56(20):4686–4693. [PubMed: 8840985]

28. Weissleder R, Stark DD, Engelstad BL, Bacon BR, Compton CC, White DL, et al. Superparamagnetic iron oxide: Pharmacokinetics and toxicity. Am. J. Roentgenol. 1989; 152:167–173. [PubMed: 2783272]

29. Wang Y-XJ, Hussain SM, Krestin GP. Superparamagnetic iron oxide contrast agents: physicochemical characteristics and applications in MR imaging. Eur. Radiol. 2001; 11:2319–2331. [PubMed: 11702180]

30. Joshi S, Emala CW, Pile-Spellman J. Intra-arterial drug delivery: a concise review. J. Neurosurg. Anesthesiol. 2007; 19(2):111–119. [PubMed: 17413997]

31. Doolittle ND, Miner ME, Hall WA, Siegal T, Jerome E, Osztie E, et al. Safety and efficacy of a multicenter study using intraarterial chemotherapy in conjunction with osmotic opening of the blood-brain barrier for the treatment of patients with malignant brain tumors. Cancer. 2000; 88(3):637–647. [PubMed: 10649259]

32. Khoo VS, Dearnaley DP, Finnigan DJ, Padhani A, Tanner SF, Leach MO. Magnetic resonance imaging (MRI): considerations and applications in radiotherapy treatment planning. Radiother. Oncol. 1997; 42(1):1–15. [PubMed: 9132820]

33. Levin CV, Hough J, Adams LP, Boonzaier D, Ruther H, Wynchank S. Determining locations of intracerebral lesions for proton radiotherapy. Phys. Med. Biol. 1993; 38(10):1393–1401. [PubMed: 8248287]

34. Takeda, S-i; Mishima, F.; Fujimoto, S.; Izumi, Y.; Nishijima, S. Development of magnetically targeted drug delivery system using superconducting magnet. J. Magn. Magn. Mater. 2007; 311:367–371.

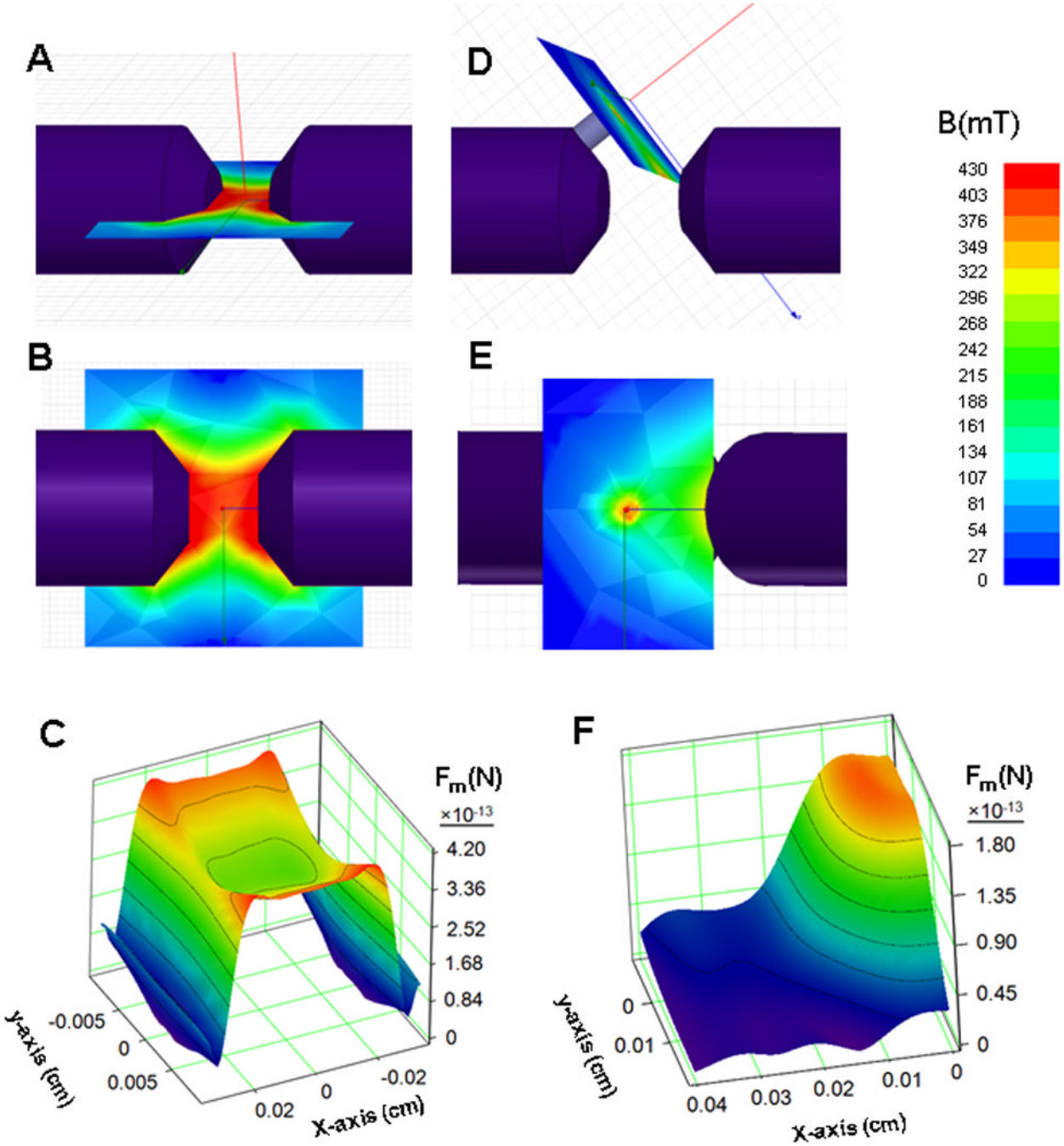

Figure 1. Design of an optimized forcefield topography via magnetic flux density simulations

Simulated magnetic flux (B) maps for a dipole electromagnet (A: top view, B: perspective view) and the optimized magnet configuration (D: top view, E: perspective view) and their corresponding calculated force fields (C : electromagnet and F: optimized configuration) acting on a single nanoparticle (F_m).

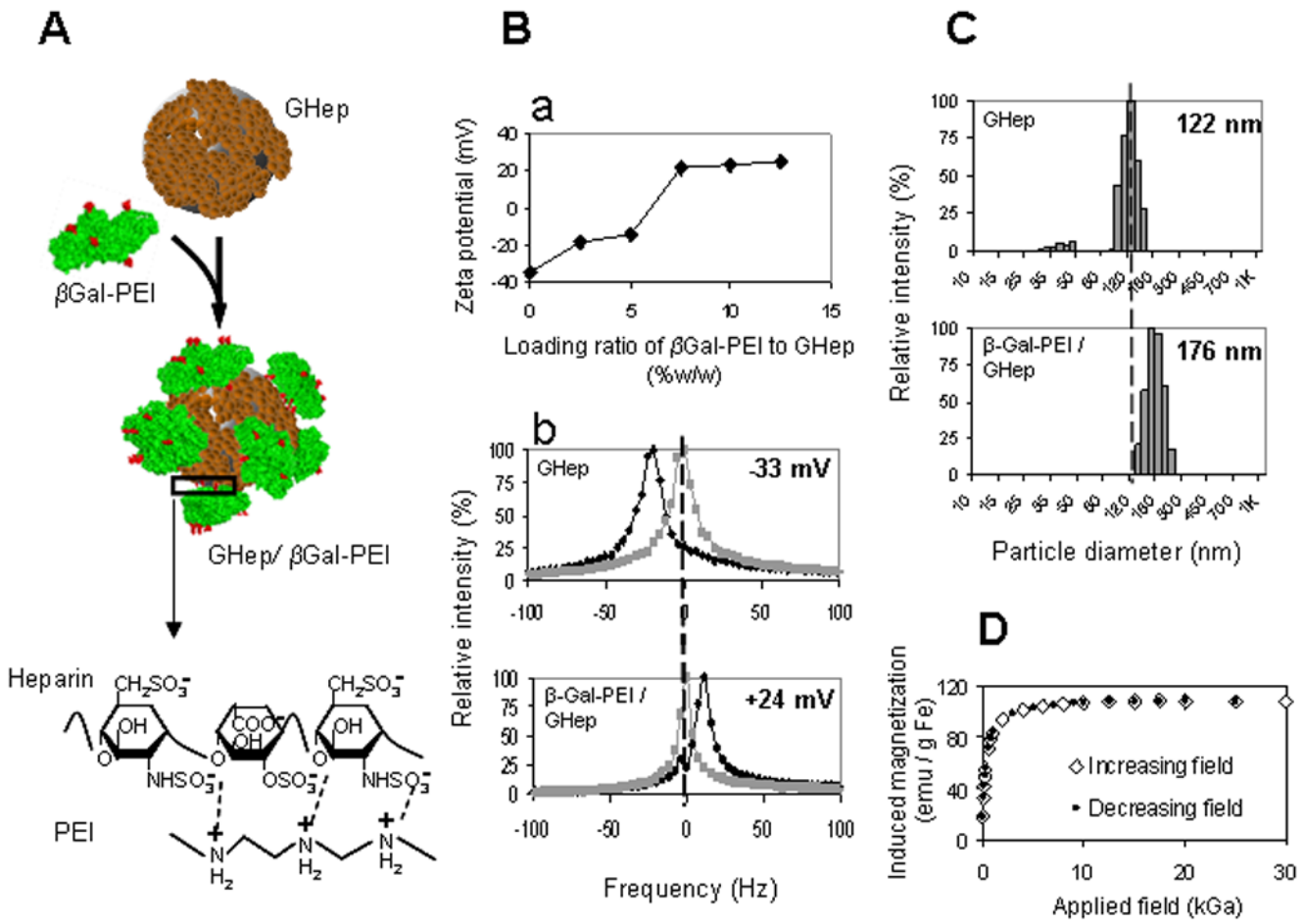

Figure 2. Characterization of protein-nanoparticle complexation

(A) PEI-modified (red) β-Galactosidase (βGal-PEI, green) is adsorbed onto the surface of heparin-coated nanoparticle (GHep, brown) to create GHep/βGal-PEI complex via electrostatic interactions between positively charged PEI and negatively charged heparin (magnified region). (Ba) ζ-potential profile as a function of βGal-PEI/GHep loading ratio exhibits saturation behavior and indicates protein loading capacity of 7.5%w/w. (Bb) Shift in ζ-potential (measured at pH=5.5) from −33 mV to +24 mV (black and gray traces represent the test and the reference measurements, acquired with and without an electric field, respectively). (C) Increase in mean particle diameter from 122 nm to 176 nm for GHep and GHep/βGal-PEI, respectively, confirm complexation. (D) Magnetization of protein-loaded nanoparticles demonstrate coinciding profiles with increasing and decreasing applied magnetic fields with no hysteresis, characteristic of superparamagnetic behavior.

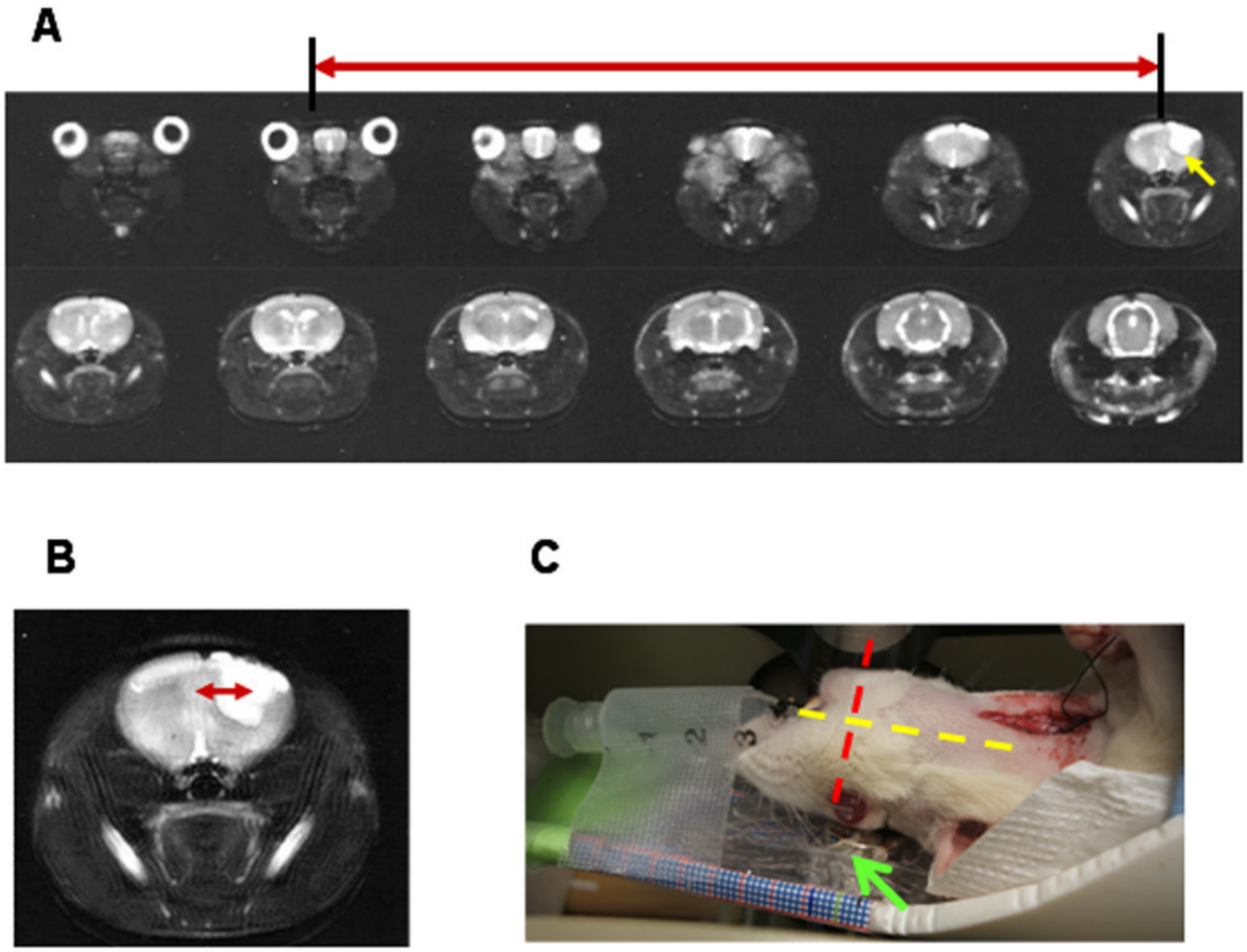

Figure 3.

Typical series of axial MRI scans (T_2-weighted) of a rat head revealing the brain localization of the tumor lesion (hyperintense region marked with yellow arrow). (A) Distance along the longitudinal dimension with respect to the middle of the eye (slice spacing X 4). (B) Distance along the lateral dimension with respect to the midline of the head. Red arrows mark the distance of the tumor lesion from the corresponding externally visible anatomical feature. (C) Image demonstrating rat alignment on the magnet (marked with green arrow) according to the MRI-derived tumor coordinates. Longitudinal and lateral dimensions are indicated with the yellow and the red dashed lines, respectively.

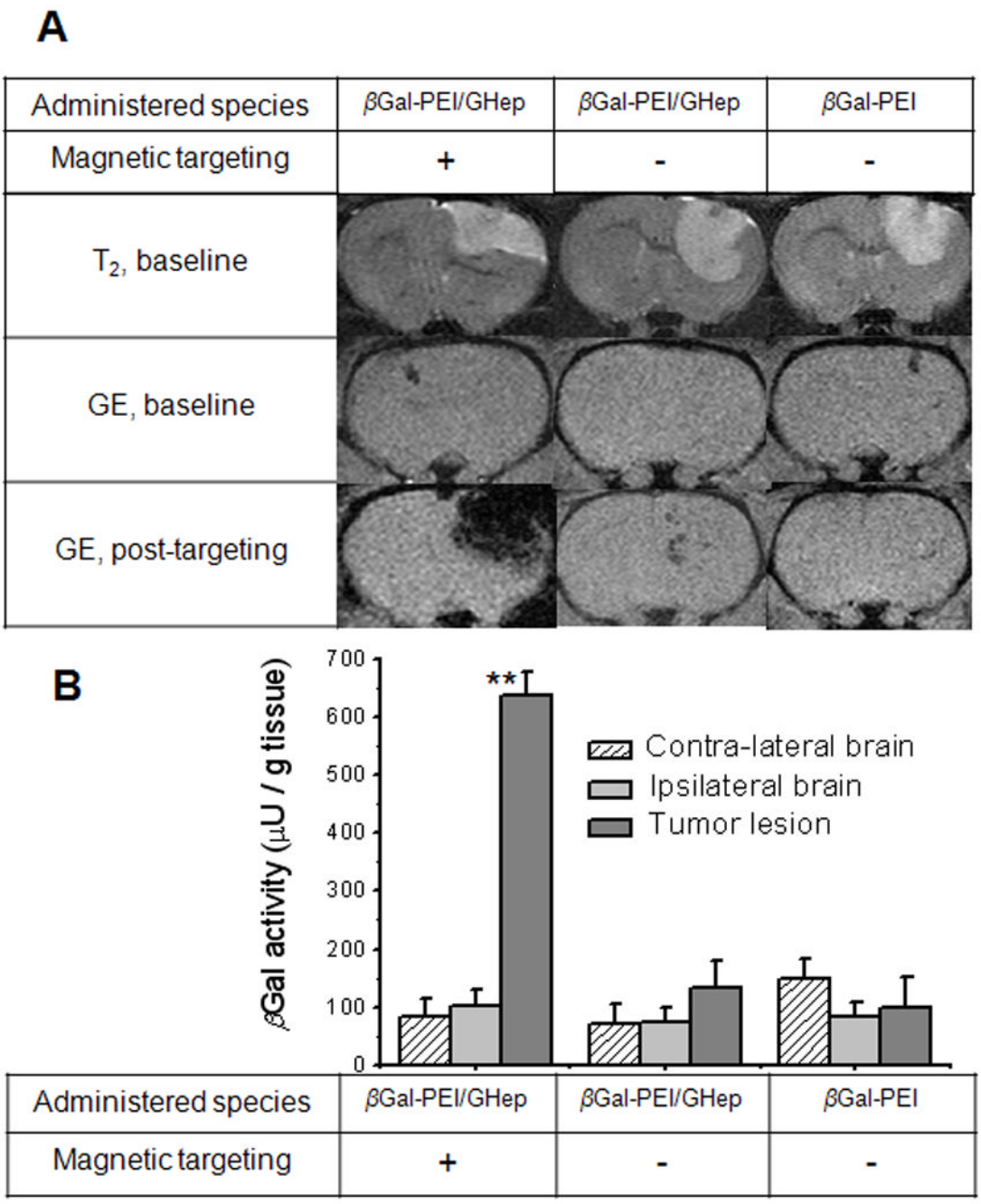

Figure 4. Delivery of βGal-PEI/GHep complexes to tumor lesions of rats harboring orthotopic 9L gliosarcomas

(A) Typical subset of MRI scans of the rat brain demonstrates nanoparticle accumulation (hypointense region on GE post-targeting scan, acquired immediately following magnetic targeting procedure) in tumor lesions (hyperintense region on T_2-weighted baseline scans) of magnetically-targeted, but not control animals. (B) βGal activity determined by CPRG assay in excised tumor and contra-lateral brain tissues of animals administered with βGal-PEI (control) or βGal-PEI/GHep complexes with (test) or without (control) magnetic targeting. Tumors of magnetically targeted rats administered with βGal-PEI/GHep complexes

exhibited significantly higher βGal activity (denoted as **) than all other analyzed samples ($p<0.001$), confirming targeted protein delivery to the tumor.

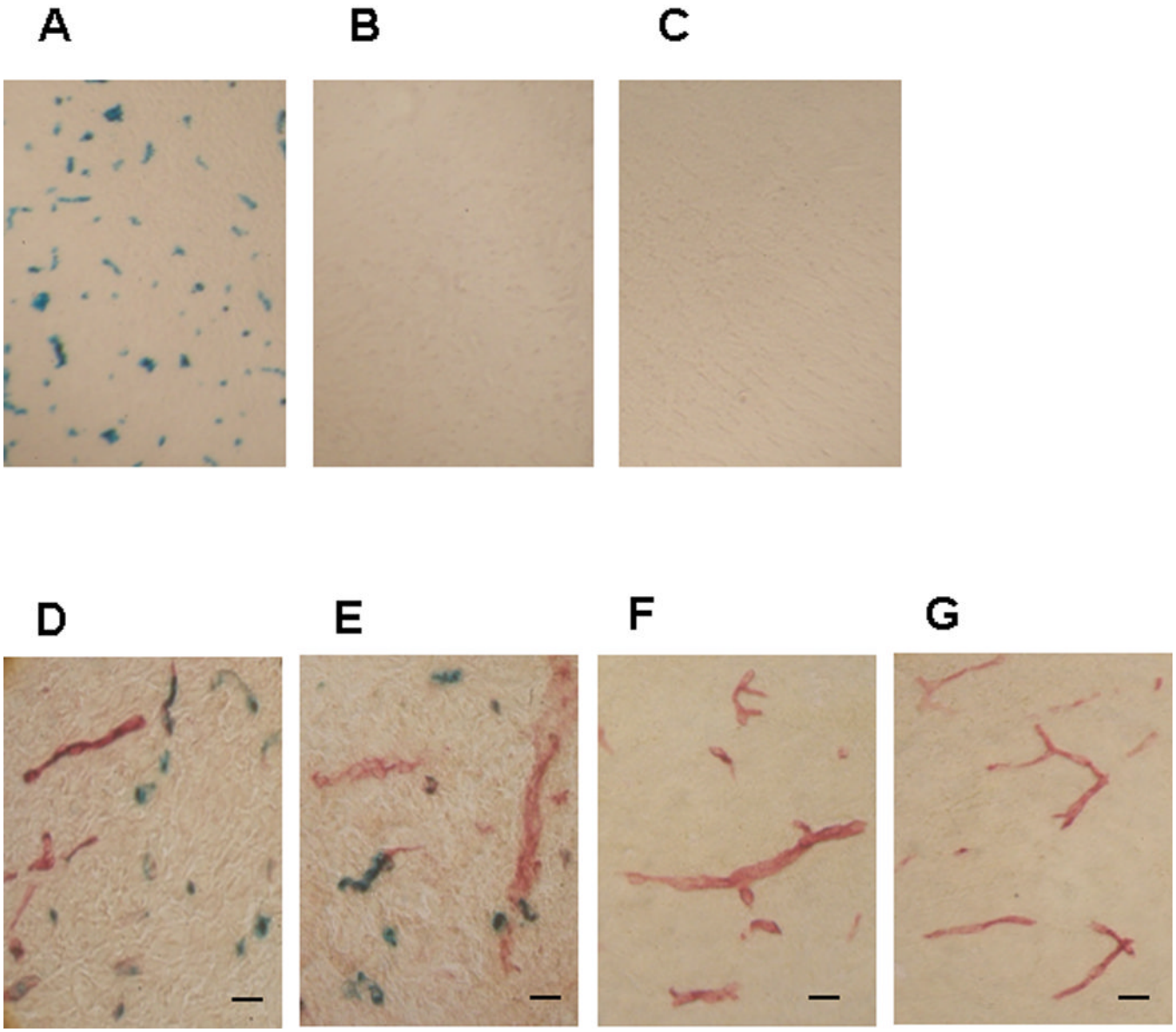

Figure 5. Histochemical analysis of βGal distribution in the brain

Representative cryosections were obtained from (A, D, E) the tumor, (B, F) the contralateral and (C, G) the ipsilateral brain regions of complex-administered magnetically-targeted rats (scale bar ~25 μ m). The sections were stained with Burstone's and X-Gal stainings to visualize localization of capillaries (red) and the delivered protein βGal (blue), respectively.

Table 1

Ratios of magnetic (F_m) to hydrodynamic (F_h) force acting on a single nanoparticle at the spatial locations of the carotid artery and the tumor lesion calculated using simulated magnetic flux density maps for the dipole electromagnet and optimized magnet configuration.

	F_m/F_h Dipole electromagnet	**F_m/F_h Optimized magnet configuration**
Carotid artery	2.7	0.4
Tumor lesion	3.4	1.8